ACS APPLIED MATERIALS & INTERFACES

Research Article

www.acsami.org

Hierarchical Composite Structures Prepared by Electrophoretic Deposition of Carbon Nanotubes onto Glass Fibers

Qi An,[†,‡] Andrew N. Rider,[§] and Erik T. Thostenson*[,†,‡,⊥]

[†]Department of Materials Science and Engineering, [⊥]Department of Mechanical Engineering, and [‡]Center for Composite Materials, University of Delaware, Newark, Delaware 19716, United States

[§]Defence Science and Technology Organization, Fisherman's Bend, Victoria 3207, Australia

Supporting Information

ABSTRACT: Carbon nanotube/glass fiber hierarchical composite structures have been produced using an electrophoretic deposition (EPD) approach for integrating the carbon nanotubes (CNTs) into unidirectional E-glass fabric, followed by infusion of an epoxy polymer matrix. The resulting composites show a hierarchical structure, where the structural glass fibers, which have diameters in micrometer range, are coated with CNTs having diameters around 10−20 nm. The stable aqueous dispersions of CNTs were produced using a novel ozonolysis and ultrasonication technique that results in dispersion and functionalization in a single step. Ozone-oxidized CNTs were then chemically reacted with a polyethyleneimine (PEI) dendrimer to enable cathodic EPD and promote adhesion between the CNTs and the glass-fiber substrate. Deposition onto the fabric was accomplished by placing the fabric in front of the cathode and applying a direct current (DC) field. Microscopic characterization shows the integration of CNTs throughout the thickness of the glass fabric, where individual fibers are coated with CNTs and a thin film of CNTs also forms on the fabric surfaces. Within the composite, networks of CNTs span between adjacent fibers, and the resulting composites exhibit good electrical conductivity and considerable increases in the interlaminar shear strength, relative to fiber composites without integrated CNTs. Mechanical, chemical and morphological characterization of the coated fiber surfaces reveal interface/interphase modification resulting from the coating is responsible for the improved mechanical and electrical properties. The CNT-coated glass-fiber laminates also exhibited clear changes in electrical resistance as a function of applied shear strain and enables self-sensing of the transition between elastic and plastic load regions.

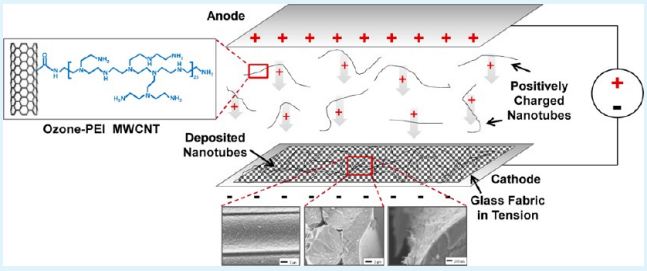

KEYWORDS: *electrophoresis, functionalization, composite, interphase, carbon nanotubes*

1. INTRODUCTION

The interface region between the reinforcing fiber and the polymer matrix plays a significant role in determining load transfer mechanisms and ultimately the strength and toughness of advanced fiber-reinforced composite materials.[1] The concept of the interphase and much of the pioneering work leading to an improved understanding of the interacting mechanisms in coatings, fillers and composites was originally reported between 1970 and 1980.[2−4] A variety of surface treatments have been applied to advanced fibers to improve fiber/matrix adhesion, and this often results in a region near the fiber/matrix interface where the properties in that region are different from the bulk polymer matrix. This region is often described as the "interphase" because of these graded material properties. In glass−fiber composites, silane coupling agents (SCA) have traditionally been used as a surface treatment to enhance bonding between thermoset-resins and glass fibers,[5−7] leading to reliable and improved composite performance.[8] Despite the simplicity of application, in which the fiber is typically treated after melt spinning with a dilute solution of a SCA, such as aminopropyltriethoxysilane (APS), the exact mechanism by which the SCA influences mechanical performance may be dependent on the specific combination of materials. Some work suggests that the interphase formed with APS and glass fiber has reduced stiffness[9] and glass transition temperatures relative to the bulk polymer matrix[10] and that the interaction of the sodium ions in the glass with the SCA film may lead to depolymerization of the siloxane network.[11] Recent modeling of the interphase region suggests that disordered interfaces facilitated by SCA addition can improve adhesion,[12] and measurements of fracture toughness for different SCA films suggest there is sensitivity to film morphology and thickness,[13] with the SCA interfacial mobility also affecting fracture toughness.[14] Clearly, there is evidence to suggest that the SCA-modified interphase in glass-fiber composites may influence toughness and strength by manipulating both adhesion and stiffness levels.

An obvious method to extend the interphase manipulation provided by SCAs is to examine incorporation of nanoscale additives at the fiber to matrix interfacial region. Nanoscale

Received: November 27, 2012
Accepted: February 4, 2013
Published: February 4, 2013

additives offer the ability to increase the matrix strength or stiffness at relatively small volume fractions by occupying the resin-rich interstitial regions between adjacent, reinforcing fibers, without increasing the overall volume of the laminate. As a result, there has been significant interest in recent years in developing hierarchical micro/nano composites where nanoscale reinforcements are integrated with traditional fibers.[15−17] Obvious nanoscale additives include graphitic based materials such as carbon nanotubes (CNTs) and graphene nanoplatelets (GNPs), which offer superior strength and stiffness for equivalent weight in comparison to more traditional materials such as alumina[18] or silica,[19] with the added benefit of high electrical conductivity and large aspect ratios. Recently, GNPs added to the epoxy resin or spray-coated directly onto the glass fibers have led to improved fatigue resistance of glass/epoxy composites due to improved interfacial toughness.[20] In a similar manner, graphene oxide combined with epoxy-based sizing-agents used to treat carbon-fibers, have also led to increases in interfacial-shear strength for single-fiber tests but showed limited increases in interlaminar shear strength of composite laminates.[21] The spray coating of CNTs onto glass fiber has also shown modest improvement in impact strength of the composite because of increases in the interfacial bond-strength at the glass−polymer interface.[22] Although pioneering research on silane coupling agents, detailed above, has provided a good grasp of mechanisms affecting interphase interactions, the addition of nanoscale additives, such as CNTs and GNPs, increases the complexity of the composite systems being designed and accurate models are still being developed.

The manipulation of the interfacial or interphase properties in glass/epoxy composites using CNTs provides great opportunities in the development of materials which can be tailored for specific applications as well as multifunctional capability. For example, controlled addition of CNTs can alter the relative conductivity of the composite and enable minimization of static charge accumulation on high speed rotating parts, provide electromagnetic interference shielding or protection from lightning-strike damage. The nanoscale additive provides wider application for the composite without weight and cost penalties associated with incorporation of heavy conductive meshes. By increasing the laminate conductivity it is also possible to incorporate a self-sensing attribute in which the conductive-CNT network can change in resistivity in response to the applied load the structure experiences.[23−26] Rausch and Mäder[27] recently utilized carbon nanotubes located at the fiber/matrix interface as sensors for detecting interphase failure or breakage of the structural fiber. If it is possible to combine the electrical benefits of the CNT-modified glass/epoxy composite with enhanced mechanical performance, there is a great incentive to develop the hierarchical, lightweight structure. For example, because of the complex nature of composite structure design applied to high speed rotating parts, often regions of laminate exist where high interlaminar stresses are generated, which leads to fracture initiation. The ability to locally strengthen the interfacial and interphase properties of the composite in these regions can lead to significant increases in shear strength and consequently much higher stresses for the onset of fracture initiation and failure. Therefore, the design of the high shear-strength regions using CNT-based hierarchical structure can be used to prevent premature failure of composites experiencing complex loading.

Although there is significant research to suggest that the incorporation of CNTs or GNPs into the interphase region of fiber reinforced polymer composites is beneficial, there is no clear indication on the best methods to efficiently disperse the nanoscale reinforcement. A variety of methods have been examined that include incorporating the reinforcement in the matrix prior to infusion of the fiber; however, this method is limited to relatively low loadings of the additive.[28,29] At high loadings of CNTs the resin viscosity increases, fabric filtering occurs and efficient dispersion becomes difficult. Typically, the measured increases in shear properties of the laminates do not exceed 30% above the baseline properties at the maximum limit of the CNT addition, which is usually around 2%.[29,30] The other disadvantage of manipulating the interphase by adding nanoscale reinforcements to the matrix is a limited capacity to tailor bonding between the fiber surface and the nanoscale reinforcement. An alternative approach to incorporating CNTs into composites involves the direct growth onto the reinforcing fiber using chemical vapor deposition.[31−33] This approach can provide perpendicular alignment of a dense forest of CNTs, which leads to improved laminate toughness and conductivity, but the heat and reaction of the catalyst with the fiber surface can degrade the overall tensile properties.[32,33] Some recent work suggests that CVD conditions may be optimized to minimize fiber degradation;[34] however, the process is energy intensive and also offers less flexibility in tailoring adhesion between the fiber and CNT. Another disadvantage of the CVD approach is that the high processing temperatures burn off existing sizing that is applied to fibers during their manufacture.

An alternative to the CVD approach is the use of electrophoretic deposition (EPD). Because of a considerable research effort in applying EPD to the development of nanoscale reinforced ceramic materials,[35] many of the significant factors leading to successful coating of conducting substrates with nanoscale materials, including CNTs, have been identified.[36,37] The benefits of EPD include the ability to scale the process to enable practical production with economical energy usage as well as greater options in the chemical design of the fiber to polymer interphase region.[38] Another benefit offered by EPD is the ability to apply relatively thick films to the fiber surface, which is more difficult to achieve with dip-coating[21] or spray-coating,[22] where lower concentration solutions are typically used to minimize viscosity increases. EPD has been applied more regularly to carbon-fiber fabrics because the conductive carbon fibers can become an electrode and an electrical potential can be applied to facilitate migration and deposition of the charged CNTs.[39,40] This original work only indicated limited increases in the mechanical properties of the composite laminates.

In the present work, we have extended the EPD method that we successfully applied to carbon/epoxy composites where we achieved a 70% increase in shear strength by treating as-sized, carbon-fiber fabric using EPD of ozone and PEI-functionalized CNTs.[41] The shear strength increase was significantly greater than previously reported for carbon/epoxy laminates treated using EPD of CNTs[39,40] and was related to improved adhesion between fiber, CNT, and epoxy as well as better through-thickness tow coating. For the first time we report the treatment of practically sized glass-fiber fabric in the as-sized condition using EPD of ozone and PEI-functionalized CNTs. Using both in-plane shear-strength tests and shear-modulus measurements, we show that considerable increases in strength result from the CNT deposited within the glass-fiber fabric prior to epoxy resin infiltration. In addition to improved strength, the CNT treatment also produces a conductive

laminate in which electrical resistance is sensitive to applied shear strain.

2. EXPERIMENTAL SECTION

2.1. Materials and Processing. Multiwalled carbon nanotubes (CM-95, Hanwha Nanotech, Korea) were oxidized using ultrasonication-ozonolysis for 16 h, followed by functionalization with polyethyleneimine ($H(NHCH_2CH_2)_{58}NH_2$, M_w 25 000, Sigma-Aldrich, USA). The sonication (Sonicator 3000, Misonix, USA) and ozonolysis (1000BT-12, Taoture International) approach, which has been described previously,[41] used a 12.7 mm diameter horn operating at 60 W. The pH of the PEI and ozone-treated MWCNTs was adjusted with glacial-acetic acid (Sigma-Aldrich) to a pH of around 6. CNT concentrations for all solutions were 1.0 g/L.

EPD of the ozone and PEI-functionalized CNTs onto the glass-fiber fabric was conducted using a fabric tensioning device, shown in Figure 1, which enabled intimate contact between the fabric and cathode to facilitate a uniform coating. The fabric tensioning device enabled the anode, cathode and tensioned fabric to be immersed horizontally in 275 mL of the CNT solution. Cathodic deposition was conducted under field strengths between 12 and 64 V cm^{-1} and deposition times between 10 and 75 min. The coated area was 800 mm^2. In some instances, γ-glycidoxypropyltrimethoxysilane (GPS) (Sigma-Aldrich) was also added to the CNT-PEI dispersion at 2 to 4 g/L and hydrolyzed for 2 h at a pH of 6 prior to coating. Two laminates used E-glass where double-sided coating was applied by reversing the fabric surface in contact with the cathode after initial deposition.

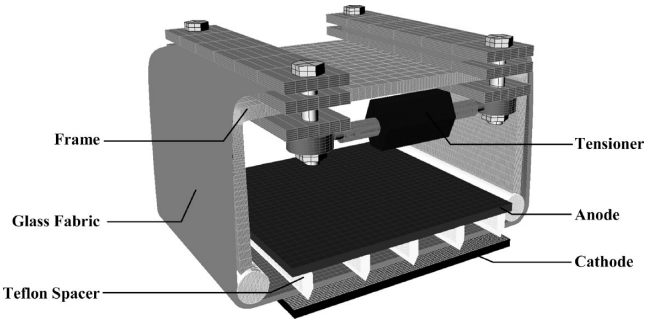

Figure 1. Experimental arrangement used to electrophoretically deposit the unidirectional E-glass fabric with CNTs. Glass fabric under tension is pressed against the cathode and the separation distance is controlled with nonconductive Teflon spacers.

2.2. X-ray Photoelectron Spectroscopy (XPS) and SEM. XPS (Kratos Nova, U.K.) of electrophoretically coated glass-fiber used a monochromatic Al $K_{\alpha,1}$ source operating at 150 W and an analysis area of 700 × 300 μm^2 with an electron flood gun to neutralize charge build-up on the insulating samples. SEM analysis (JEOL JSM-7400F and LEO 1530VP) of the coated glass-fiber and fracture surfaces of the failed glass/epoxy laminates used a 3 kV accelerating voltage with either a 5 nm Pt/Au or 1.5 nm Ir layer to prevent charging.

2.3. Dynamic Mechanical Thermal Analysis (DMTA). DMTA of glass/epoxy laminates with the CNT treatments used a Polymer Laboratories DMTA Mk III. Samples were tested in single cantilever bending (0.1% strain, 1 Hz) using a temperature ramp rate of 5 °C/min to measure the glass transition temperature (T_g) of the matrix from the onset of the decrease in storage modulus over a 60 to 250 °C range.

2.4. Composite Manufacture. Four plies of the as-received, E-glass, unidirectional fabric (style 7721, 203 g/m^2, APS sizing, Thayercraft Inc., USA) were electrophoretically deposited with ozone-PEI CNTs and dried under vacuum using semipermeable membrane (Gore Technologies, USA). The coated fabric was infused with an epoxy resin and amine curing agent (EPON 862 and Epi-Kure W, Hexion Specialty Chemicals) using vacuum assisted resin transfer molding (VARTM) with a ratio of 100/26.4. Infusion over several hours used full vacuum (−100 kPa) at 55 °C, with flow media to aid through-thickness resin diffusion, before final cure at 130 °C for 6 h. Two uncoated, E-glass/epoxy laminates were prepared separately and bonded to either side of the CNT laminate using EA9309.3 NA adhesive (Henkel, USA) followed by cure and machining of notches to the midpoint of the CNT-treated laminate (see the Supporting Information, Figure S1). Baseline laminates were prepared identically without CNT coating the 4-ply inner glass laminate. The influence of the PEI alone was also examined by using identical EPD conditions to those for the CNT coating but without CNTs present.

2.5. Mechanical Characterization. The in-plane shear strength of glass/epoxy laminates was determined based on ASTM D3846-02.[42] The in-plane shear modulus, G_{12}, of the CNT coated E-glass fabric was measured based on ASTM D3518-01[43] and used 6-ply laminates where the glass fabric was electrophoretically coated with CNTs using the same processes as described above. Shear strain was monitored using biaxial-strain gauges and the elastic region was determined from 2000 $\mu\varepsilon$ to 6000 $\mu\varepsilon$. The composite compositions were established from density measurements[44] and sulfuric-acid digestion[45] or measurement of optical cross sections of the laminate after fabrication. A minimum of five specimens were tested for each composition. The volume fraction of PEI was calculated on the basis of the ratio of CNT to PEI determined from XPS (Table 1) and was typically 1.2 times the volume of the CNTs. The concentration of PEI was a consistent ratio of the CNT concentration, which depended on the deposition field and time.

Table 1. Elemental Concentrations for EPD Films of CNTs Functionalized by Ozone, PEI, and GPS

	atomic concentration (%)			
treatment	O 1s	N 1s	C 1s	Si 2p
CNTs	0.55	0.00	99.29	0.00
OZONE[a]	11.39	0.00	87.00	0.18
OZONE-PEI[b]	10.61	13.88	73.98	0.40
OZONE-PEI-GPS[c]	11.88	12.24	73.66	1.10

[a]Trace levels of Fe, Mo, Na, Al, F. [b]Trace levels of Fe, Mo detected. [c]Trace levels of Fe, Mo, Cl and Al.

2.6. Electrical Characterization. Electrical resistance measurements for the in-plane shear samples were measured using the four-wire technique with a Keithley 6430 sub femtoamp remote sourcemeter with a constant source voltage of 20 V (ASTM D257−07[46]). Surfaces were polished and coated with silver paint prior to application of electrodes using conductive silver epoxy resin. Electrical and mechanical measurements were recorded simultaneously using a customized data acquisition system.

3. RESULTS AND DISCUSSION

3.1. Chemical Characterization. Changes in the surface chemical composition of the electrophoretically deposited CNTs after ozone, PEI and GPS functionalization are shown in Table 1. The major changes are associated with an increase in oxygen and nitrogen due to the ozone and PEI treatments, respectively. However, only a small increase in silicon is observed for addition of the GPS added at 4 g/L. C 1s photoelectron spectra (see the Supporting Information, Figure S2) also showed that there was no clear change in the film chemistry through addition of the GPS but the reaction of the PEI and ozone treated CNTs is clear, showing a significant increase in the C═O/C═N component (see the Supporting Information, Table S1). Previous studies on electrodeposition of SCAs suggest they should deposit cathodically, primarily as a result of electrolysis of water at the cathode leading to alkaline pH facilitating siloxane formation of the cationic silane.[47,48] Potentially, the hydroxyl groups generated by the electrolysis of

water at the cathode are consumed by the cationic PEI-dendrimer, which was reacted initially with the oxidized CNTs. The high electrophoretic mobility of the ozone, PEI-CNTs (+50 mV[49]), may reduce the relative concentration of the GPS molecules available to react at the cathode. Research examining the reaction of GPS with APS treated titania suggests that the zeta-potential can be slightly negative at a pH around 6,[50] which may imply that any ozone PEI-CNTs bonded to GPS would not deposit efficiently at the cathode.

The elemental concentrations of the E-glass surfaces before and after electrophoresis using the individual components of the CNT dispersion, without the CNTs present, are shown in Table 2. Nitrogen on the as-received E-glass surface is due to

Table 2. Elemental Concentrations for E-Glass Fabric before and after EPD with Deionized Water, PEI, and GPS

	atomic concentration (%)						
sample	B 1s	C 1s	N 1s	O 1s	Al 2p	Si 2p	Ca 2p
E-Glass[a]	2.57	26.99	3.18	44.39	4.51	14.22	3.37
H_2O EPD of E-Glass[b]	1.75	31.11	3.53	42.67	3.80	14.41	2.39
PEI EPD of E-Glass[c]	0.88	38.88	8.71	33.62	3.42	12.01	1.81
GPS EPD of E-Glass[d]	1.47	32.30	3.85	41.53	4.04	13.95	2.23

[a]Trace Na, F, Mg. [b]Trace Mg. [c]Trace Na, Mg. [d]Trace F, Mg.

the APS sizing agent. EPD in deionized water, with the pH adjusted to 6 with glacial acetic acid, shows no obvious changes in surface composition of the sized E-glass, suggesting that under the conditions of electrophoresis used the APS film remains adhered to the E-glass. Previous work examining the influence of moisture exposure on APS treated glass[51] suggests that the zeta-potential and interphase properties remain fairly constant, which is consistent with the data in Table 2. EPD of the PEI solution at pH 6 shows a clear increase in the nitrogen and carbon levels due to adsorption of the dendrimer. The comparatively unchanged silicon concentration from the glass substrate suggests that the film is less than the Si 2p photoelectron escape depth, estimated to be between 3 and 5 nm. However, it should be noted that an inhomogeneous coverage or cross-link density of the APS film could also provide a similar photoelectron response and, therefore, may also be possible. The electrophoresis in GPS at pH 6 suggests that minimal deposition occurs, given the similar elemental concentrations to the as-received E-glass and the E-glass after EPD in water. This is consistent with the CNT film (Table 1), where only small increases in silicon were observed when GPS was added to the solution.

Figure 2 shows the N 1s photoelectron peaks for the E-glass fiber after EPD in deionized water and PEI at pH 6, compared to the ozone and PEI-functionalized CNT film. The peaks between 399.8 and 400.1 eV are attributed to the amine bonding in the APS (peak III, Figure 2a) or PEI[52−54] (peak III, Figures 2b&c). The significant peak for the PEI film electrophoretically deposited on E-glass (peak IV, Figure 2b) is at 1.0 eV lower than the amine peaks and may suggest chemical reaction of the dendrimer and glass or change to the PEI chemical structure resulting from EPD. The ozone and PEI-functionalized CNT film exhibits a low binding energy peak (peak V, Figure 2c), at 398.0 eV and a high binding energy peak at 402.5 eV (peak I, Figure 2c), which may indicate

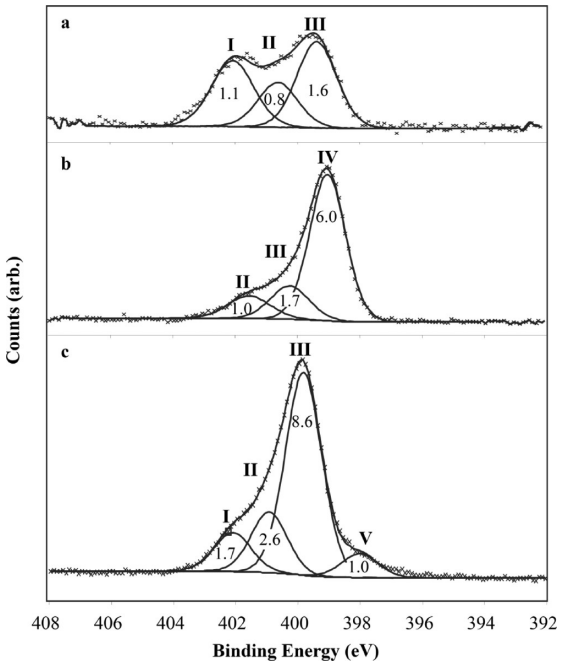

Figure 2. N 1s photoelectron spectra for E-glass fiber after EPD at pH 6 in (a) deionized water, (b) 1g/L PEI solution, and (c) ozone and PEI functionalized CNTs (atomic concentrations labeled).

pyridinic and oxidized-pyridine structures,[55] because of chemical interaction between the PEI and oxidized CNTs.

3.2. Nanotube Deposition. The deposition mass for the ozone and PEI-functionalized-CNT dispersion at field strengths between 12.5 and 64 V cm^{-1} is shown in Figure 3a. In the initial linear deposition stage it was possible to estimate the rate dependence on field strength (Figure 3b). The deposition rate is compared to that measured for carbon fibers in previous work.[41] As can be seen the deposition rate at the same field strength is about the same as on carbon where the solution concentration was only 0.5 g/L. On the basis of the linear dependence of deposition rate with dispersion concentration, estimated from the Hamaker equation,[56] the results in Figure 3b suggest that the deposition rate on glass is around half that observed on carbon fibers. The reduced rate may be expected as the film deposition process on glass would differ to a conducting substrate. Initially, the shielding of the cathode by the glass fabric could reduce the effective field-strength and deposition of the functionalized CNTs may be expected to be driven initially by precipitation resulting from high-localized pH caused by electrolysis of the water. Previous studies on EPD of PEI have suggested that high pH gradients at the cathode may lead to destabilization of the dispersion and consequent precipitation.[57] Once a sufficient quantity of CNTs precipitates onto the glass fibers and reaches the electrical percolation threshold the glass then behaves like a conductive substrate.

3.3. Film Characterization. Figure 4 shows CNTs deposited on the E-glass fiber from the CNT dispersion at 25 V/cm for 15 min. The film appears to be compact with the CNTs embedded in the PEI polymer. The outer surface of the fabric (Figure 4a, b) shows a uniform film around 2 μm thick. Deeper into the fabric tow (Figure 2c, d), the film appears to reduce with thicknesses between 50 and 200 nm. This trend in thickness suggests that once the fiber bundles reach electrical percolation and become conductive the film builds up at a faster rate on the fibers on the outer surface of the fabric.

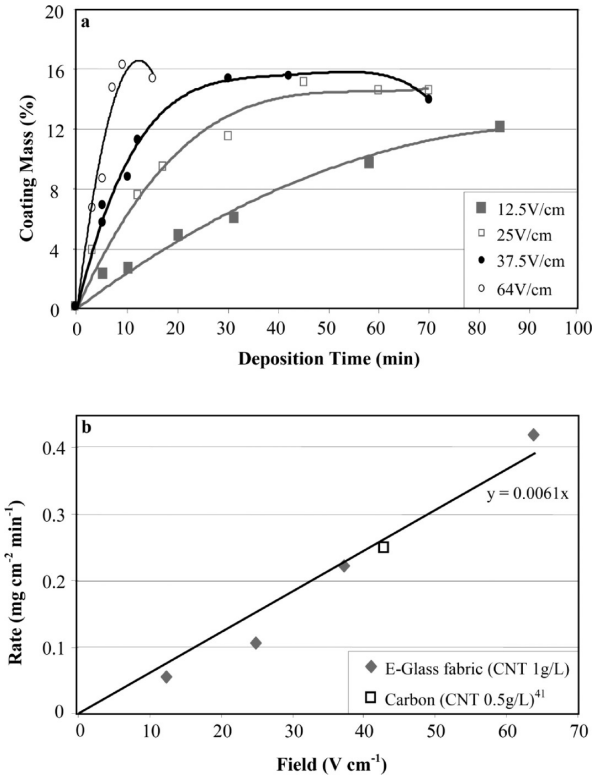

Figure 3. (a) Mass change of E-glass fabric as a function of deposition time in 1g/L CNT solution with different field strengths and (b) film deposition rate as a function of field strength for E-glass and carbon-fiber fabric[41].

Polished cross-sections of the epoxy-infused glass-fibers with CNTs deposited were also examined to determine porosity and CNT distribution throughout the laminate (Figure 5). The film that builds up on the outer fibers appears to be well infused (Figure 5a) and there are few voids, even when observed at high magnification (Figure 5b), indicating the resin diffuses through the coating and produces a good-quality, low-void laminate. Further into the interior of the fabric, the coating thickness decreases and a thin CNT coating is observed around individual fibers together with a network that spans between adjacent fibers (Figures 5c,d). Optical images acquired using transmitted light of thin laminate sections (see the Supporting Information, Figure S3) show the coating is present throughout the thickness, suggesting that the network structure observed in images c and d in Figure 5 occurs along the length of the fibers and throughout the composite.

3.4. Thermal Analysis. Table 3 shows the T_g values for E-glass fibers coated with CNTs prior to preparation of laminates used to measure the in-plane shear modulus, G_{12}. The results indicate the CNTs and PEI have minimal effect on the T_g of the resin system. Previous work examining addition of PEI to epoxy resin suggests that the dendrimer branches can facilitate high cross-link density bonds at only 2.5−5% addition;[58] however, the results in Table 3 suggest that in combination with the CNTs, there is not an obvious increase in the cross-link density of the epoxy resin. The result is more favorable than has been reported for addition of polyamido-amine dendrimers (PAMAM-O) to epoxy-CNT mixtures, where a decrease in T_g was attributed to the PAMAM-O inhibiting the epoxy cross-linking reaction.[59] At the high-volume fractions of PEI and CNTs in the matrix, the unchanged T_g in Table 3 suggests that the functionalized CNTs may not have affected the epoxy cross-linking reactions. However, it should be noted that, as the total volume of the interface between the epoxy and functionalized CNTs may be relatively small, it may not be possible to resolve T_g changes in this highly localized region

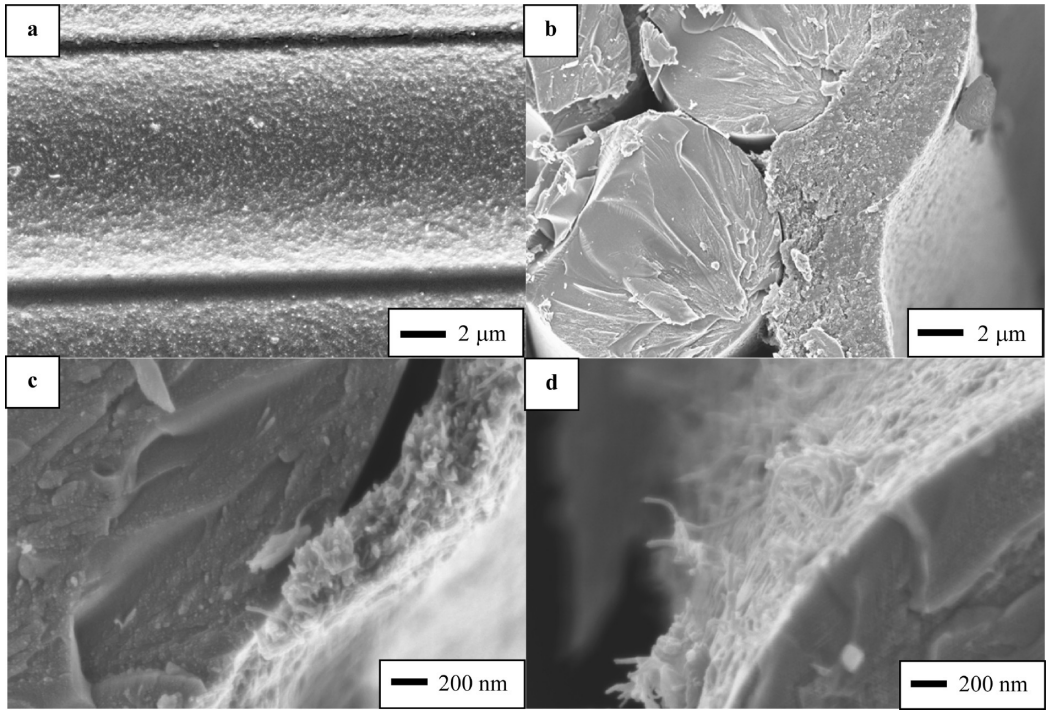

Figure 4. SEM images of the E-glass fiber after EPD coating with the ozone and PEI-functionalized CNTs indicating (a) the outer fiber surface, (b) a cross-section through the outer coating, (c, d) coating toward the fiber-tow interior.

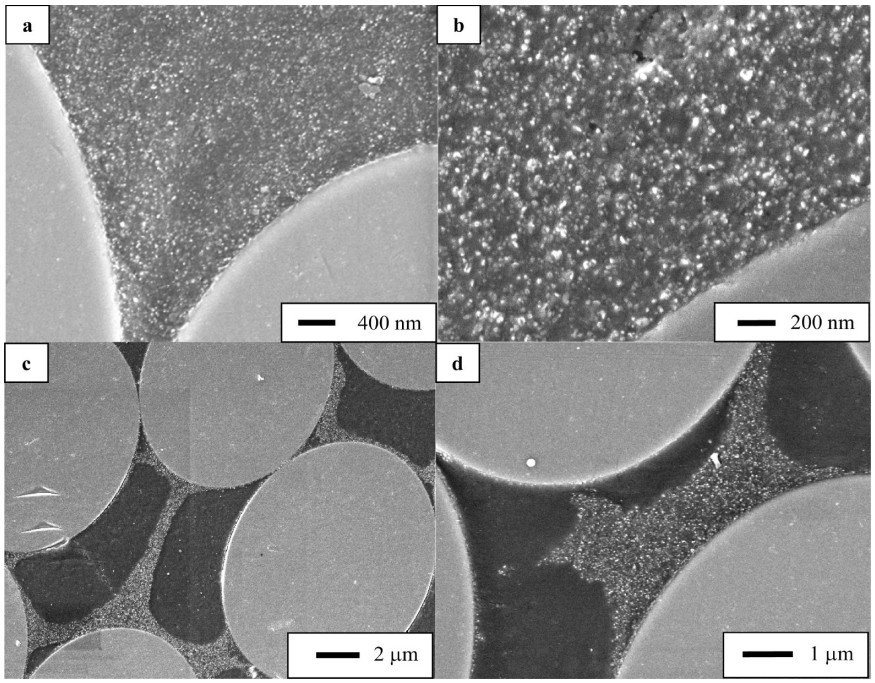

Figure 5. SEM cross-sectional images of the E-glass fabric after CNT coating and epoxy resin infusion showing (a, b) the outer fiber surface and (c, d) the distribution of coating for the interior fibers.

Table 3. DMTA Results for ±45° CNT-Treated E-Glass/Epoxy Laminates Indicating Volume Fraction of CNTs (V_{CNTs}) and PEI (V_{PEI}) in the Matrix (V_m)

	baseline	±45° CNT-1	±45° CNT-2	±45° CNT-3	±45° CNT-4	±45° CNT-5
V_{CNTs}/V_m (%)	0	14	12	9	9	6
V_{PEI}/V_m (%)	0	17	14	10	11	8
T_g (°C)	142	141	138	142	141	142

using the current experimental arrangement. Future experiments may require techniques such as nanoindentation to resolve the level of cross-linking at the localized interface between the CNT and epoxy resin or measurements on bulk nanotube/epoxy composite films where a model composite is produced that mimics the localized structure of the interphase region.

3.5. In-Plane Shear Strength. The composition of E-glass/epoxy laminates in which the fiber was electrophoretically coated with CNTs or PEI prior to resin infusion is shown in Table 4. The volume fraction of CNTs and PEI was estimated from the density of the matrix and based on the ratio of CNT to PEI determined from XPS (Table 1). The results indicate that double-sided coating at medium field strengths (DN-EPD-CNT-5 and 6) produced laminates with high volume fractions of CNT and PEI but also reduced the fiber volume fraction (V_f) relative to the baseline laminate. The reduced V_f is associated with a thicker outer film (Figure 4) and slight increase in the interlaminar-layer of around 20 μm for DN-EPD-CNT-5 compared to 10 μm for the baseline (see the Supporting Information, Figure S3). Interestingly, the highest CNT volume fraction (V_{CNTs}) was estimated for DN-EPD-CNT-7, which used single-sided coating, the lowest field strength and longest coating time. Additionally, the volume of solution used was about 50% greater than the other samples. Although the V_{CNTs} was highest for DN-EPD-CNT-7, the V_f was higher than the two samples prepared using double-sided coating (DN-EPD-CNT-5 and 6) and the interlaminar-layer was around 15 μm (see the Supporting Information, Figure S3). This suggests that the deposition conditions may have produced a more homogeneous coating within the glass fabric, leading to better laminate consolidation.

Table 4. Composition of In-Plane Shear, CNT-Treated E-Glass/Epoxy Samples Indicating Fiber (V_f), Epoxy (V_E), CNT (V_{CNTs}), and PEI (V_{PEI}) Volume Fractions[a]

laminate	field (V cm^{-1})	time (min)	$\%V_f$	$\%V_E$	$\%V_{CNTs}$	$\%V_{PEI}$
baseline	0	0	53.5 (1.4)	46.0 (1.4)	0	0
DN-EPD-PEI[b,f]	25	12	53.6 (0.9)	46.0 (1.0)	0	<1
DN-EPD-CNT-1	36	40	60.5 (0.4)	36.2 (0.4)	1.2 (0.6)	1.5 (0.6)
DN-EPD-CNT-2	55	30	53.4 (0.3)	40.8 (0.4	2.4 (0.7)	2.9 (0.7)
DN-EPD-CNT-3	36	60	49.8 (0.5)	35.8 (0.6)	6.4 (1.3)	7.6 (1.3)
DN-EPD-CNT-4	54	20	53.7 (0.9)	31.6 (0.9)	6.5 (1.4)	7.7 (1.5)
DN-EPD-CNT-5[b,c]	38	8	39.1 (0.4)	40.7 (0.5)	8.8 (0.9)	10.4 (0.9)
DN-EPD-CNT-6[b,d]	25	12	42.1 (0.7)	37.6 (0.7)	8.8 (1.2)	10.5 (1.2)
DN-EPD-CNT-7[e]	18	90	46.4 (0.8)	22.0 (0.9)	14.2 (1.5)	16.9 (1.6)

[a]Standard deviations are shown in parentheses. [b]Fabric coated both sides. [c]2 g/L GPS added. [d]4 g/L GPS added. [e]Dispersion volume 400 mL per fabric layer. [f]EPD with 1 g/L PEI only.

Figure 6 shows a plot of the in-plane shear strength as a function of V_{CNTs}. The strength increases in direct proportion

dx.doi.org/10.1021/am3028734 | ACS Appl. Mater. Interfaces 2013, 5, 2022−2032

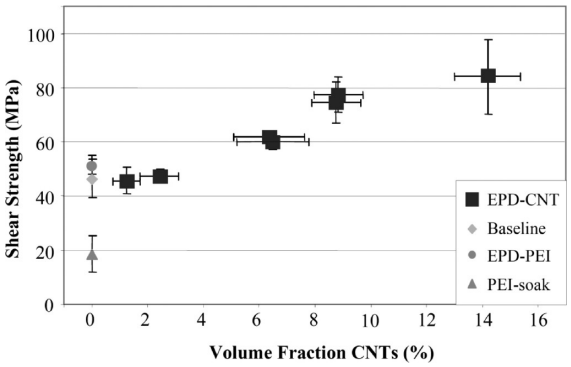

Figure 6. In-plane shear strength measured for E-glass/epoxy laminates where the E-glass was electrophoretically coated with ozone and PEI-functionalized CNTs prior to resin infusion.

to the CNT concentration and leads to an 80% increase in strength for the highest V_{CNTs} compared to the baseline. The laminate prepared using EPD of PEI produces a small increase in the baseline strength, which suggests that the PEI creates a favorable bond between the APS-sized glass and the epoxy resin. The PEI-soaked laminate led to a lowering of the strength, which implies that the EPD process alters the PEI chemistry favorably for bonding. The results presented in Figure 6 show that a significant loading of CNTs and PEI results in significant increases in the shear strength. Previous increases reported in the literature for nanoscale carbon additions are around 10−15% for practical-scale shear tests.[21,39,40] The difference between the current work and that previously reported are the higher volume-fraction of CNTs used and the incorporation of PEI at relatively high levels. The combined sonication and ozonolysis approach, which helps to reduce agglomeration of the CNTs, assists in depositing a very uniform coating and, potentially, the PEI provides a toughening component that helps to reduce the influence of stress concentrations generated at the coating and resin interphase regions. Previous work suggests that PEI can increase epoxy toughness by 30−40%[58] and our prior research on EPD treatment of carbon fibers with PEI-functionalized CNTs led to an 80% increase in carbon/epoxy mode I fracture toughness.[41]

As the CNTs and PEI are a consistent ratio in the different laminates, it is difficult to definitively establish the relative contribution of the CNTs and PEI to the strength improvements observed. Although it appears that the PEI alone provides a small increase in glass-epoxy adhesion strength (Figure 6), at volume fractions greater than 6%, the shear strength increases are mainly due to greater matrix stiffness and strength. Previous work in which PEI was directly mixed into epoxy resin[58] at 5% indicated relatively small increases in modulus and strength, which would imply the CNTs are primarily responsible for the improved shear strength. However, it is clear that further research is required where the relative ratios of the ozone-functionalized CNTs and PEI could be altered to provide a better measure of their relative contributions to the observed improvements in mechanical properties.

The results in Figure 6 also indicate that the addition of GPS does not lead to any obvious increases in strength. The two laminates around 9% V_{CNTs} have 2 and 4 g/L of GPS added, but the overall trend in strength is similar to other laminates where GPS was not used. This is consistent with the XPS analysis (Table 2) and suggests that the PEI is sufficient to achieve strong bonding to the sized glass-fiber and epoxy resin via the functionalized CNTs.

SEM images of the baseline laminate (Figure 7a, b) and DN-EPD-CNT-6 laminate (Figure 7c−e) show the fracture surfaces for the failed in-plane-shear specimens. The baseline fracture occurs at the fiber and resin interface and the resin exhibits brittle fracture of the epoxy resin. The fiber surfaces also show thin-localized islands of resin where some failure in the resin interphase has occurred. The fracture suggests that the strength is strongly influenced by the adhesion strength at the glass−epoxy interface and affected by a thin, heterogeneous, resin-interphase region. In contrast, the DN-EPD-CNT-6 laminate fracture surface reveals that a thin, CNT-rich, resin-layer coats the fiber surface (Figure 7d, e) and the region between the fibers (Figure 7f) also contains CNTs, which appear to have changed the fracture morphology from a brittle to a more ductile appearance. There are also very few cases where exposed CNTs can be observed, suggesting that the bond strength between the functionalized CNTs and epoxy is not a factor limiting adhesion strength at the fiber−matrix interphase. The shift in fracture path from the interface into the CNT-rich interphase also indicates that good adhesion between the functionalized CNTs and APS coated fibers is established.

3.6. In-Plane Shear Modulus. The composition of ±45° E-glass/epoxy laminates with the CNT treatment is shown in Table 5. The E-glass was treated in a similar manner to the DN-EPD-CNT-6 laminate (Table 4). The volume fraction of CNTs (V_{CNTs}) follow the expected trend based on the location from which the samples were cut, with ±45° CNT-1 and 2 taken from the middle and ±45° CNT-3 to 5 from the outer coated areas, respectively. The volume fractions of CNTs for the in-plane shear (DN-EPD-CNT-6) and the shear modulus samples (±45° CNT-1) are relatively similar, indicating reasonable reproducibility for the EPD coating method. Most of the ±45° CNT samples have similar V_f, which is not significantly lower than the baseline laminate, therefore, a reasonable estimate of the influence of the EPD-CNT treatment on shear modulus is possible.

Figure 8a shows the measured shear modulus (G_{12}) for CNT treated E-glass/epoxy laminates generally increases with the volume of CNTs in the matrix (V_{CNTs}/V_m), where V_m is equal to the sum of V_E, V_{CNT}, and V_{PEI}. However, there is a slight decrease for the highest concentration of CNTs. The maximum increase in modulus relative to the untreated laminate is around 30% at about 12% V_{CNTs}/V_m. The anticipated increase in shear modulus was also examined with the widely used Halpin−Tsai equations,[60] which were modified for 3D random-alignment of the CNT reinforcement in the matrix.[61] The modeling assumed the CNT coating was a constituent of the resin and the volume fraction was used to estimate the shear modulus of the matrix, G_{random}, based on the aspect ratio of the CNTs (l_f/d_f). The equations used for modeling are detailed in the Supporting Information, as are the material property data.

Figure 8b shows G_{random} values used in the periodic microstructure model,[62] which are required to match the measured G_{12} data in Figure 8a. Using the known CNT concentrations corresponding to the G_{random} values, a comparison with the 3D random CNT model can be made by assuming different filler aspect-ratios. The results show that if the CNT aspect ratio is assumed to be around 10 there is some agreement with the model for the three lowest CNT concentrations, however, at the highest concentrations the

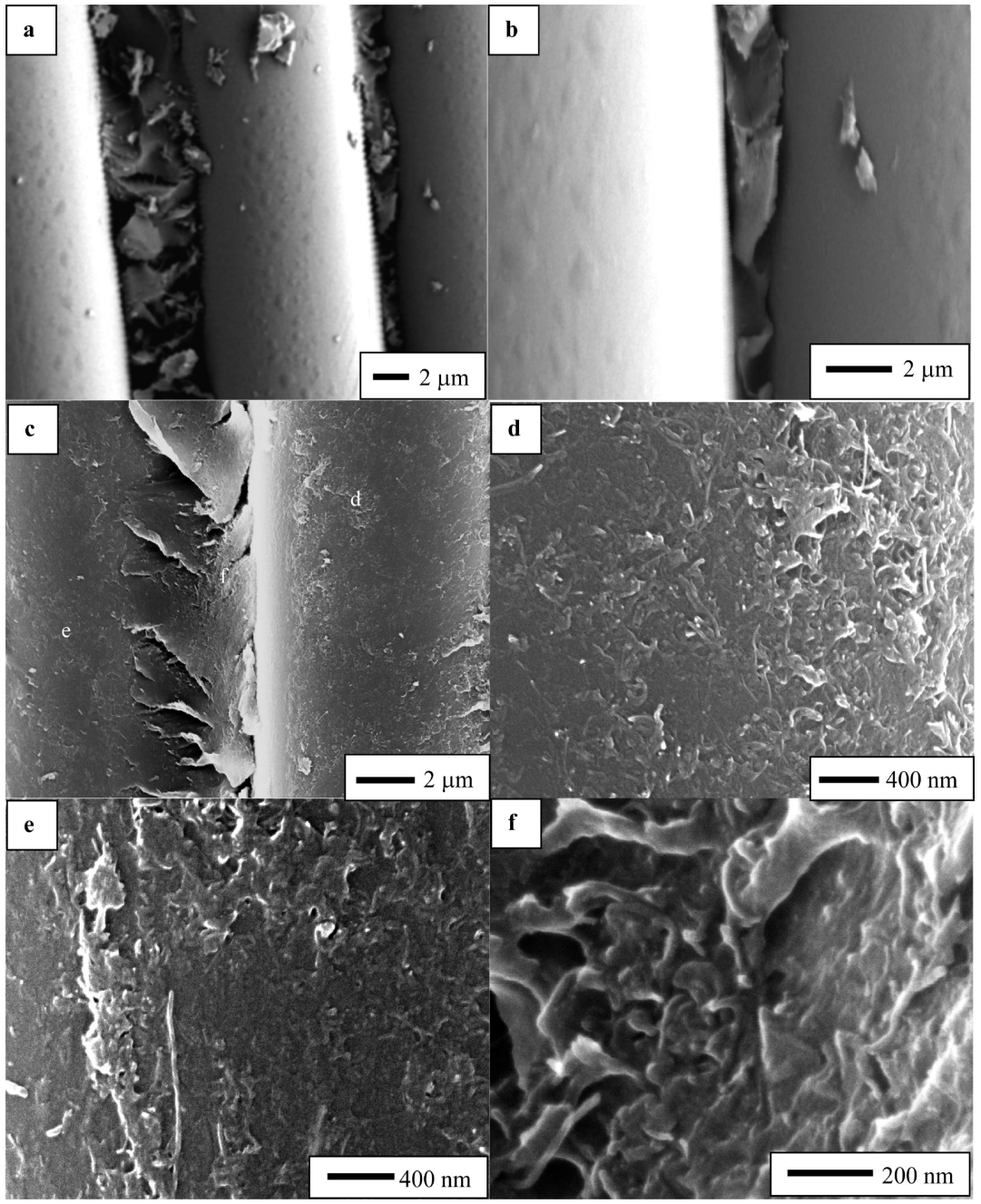

Figure 7. SEM images of (a, b) baseline laminate and (c−) DN-EPD-CNT-6 laminate (Table 4) indicating the shear fracture surfaces. Higher-magnification images (d, e) on the adjacent fibers and (f) in the matrix-rich zone between the fibers indicate a CNT-rich resin layer.

Table 5. Composition of CNT-Treated E-Glass/Epoxy ±45° Laminates Indicating Fiber (V_f), Resin (V_E), CNT (V_{CNTs}), PEI (V_{PEI}) and Void (V_v) Volume Fractions[a]

laminate	$\%V_f$	$\%V_E$	$\%V_{CNTs}$	$\%V_{PEI}$	$\%V_v$
baseline	49.4 (0.5)	47.9 (0.5)	0.0	0.0	2.8 (0.5)
±45° CNT-1	46.6 (0.6)	35.0 (1.2)	7.1 (1.3)	8.4 (1.3)	2.9 (1.3)
±45° CNT-2	47.6 (0.8)	36.6 (1.4)	5.8 (1.2)	6.9 (1.4)	3.1 (1.4)
±45° CNT-3	46.2 (0.5)	43.2 (1.0)	4.7 (1.0)	5.6 (1.0)	0.3 (1.1)
±45° CNT-4	43.6 (0.4)	46.0 (0.8)	4.7 (0.8)	5.7 (0.9)	0.0 (0.9)
±45° CNT-5	45.5 (0.5)	46.7 (0.9)	3.4 (1.1)	4.1 (1.2)	0.3 (1.3)

[a]Standard deviations shown in parentheses.

shear modulus values drop well below the values predicted for a reasonable CNT aspect ratio. It should also be noted that the elastic modulus of the CNTs used a value around 200 GPa, which is only half that used in previous modeling studies for

dx.doi.org/10.1021/am3028734 | ACS Appl. Mater. Interfaces 2013, 5, 2022−2032

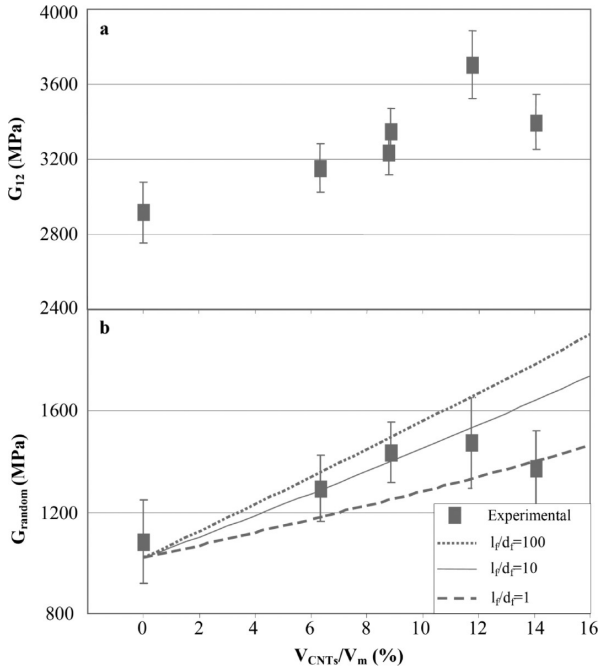

Figure 8. (a) Shear modulus (G_{12}) measured for the CNT-treated E-glass/epoxy composite and (b) the effective shear modulus of the CNT-modified matrix (G_r) compared to the Halpin−Tsai equation for different aspect ratios (l_f/d_f) of the 3D randomly oriented CNTs.

multiwalled CNTs,[63] to allow for structural damage that may be caused during the sonication. The aspect ratio of 10 is also conservative, as the average CNT diameter is around 15 nm and lengths for functionalized CNTs shown in Figures 4 and 7 and previous work[41] are greater than 200 nm.

Therefore, the Halpin−Tsai model overestimates the shear modulus increase expected for the concentration of CNTs present, which may be related to the inhomogeneous distribution of CNTs throughout the matrix, as shown in Figures 5c, d. Potentially, the modulus increase at the lower CNT concentrations represents the improvement in the load transfer between the fiber and matrix afforded by the thin-film coating of the fibers and regions where the film has established a network between the fibers. At higher concentrations, the coating on the outer-fibers of each ply may thicken but the coating on the inner-fibers and between the fibers may not increase sufficiently to affect the matrix stiffness or load transfer mechanisms (Figure 4). The total laminate stiffness then does not increase at the rate expected for the case where CNTs are homogenously distributed throughout the matrix.

3.7. Electrical Properties. The volume conductivity for the CNT treated E-glass/epoxy laminates is shown in Figure 9 for measurements taken parallel and normal to the fiber direction. A fit to the data used the classical equation from percolation theory[64]

$$\sigma = \sigma_o(p - p_c)^t \quad (1)$$

where σ is the volume conductivity, σ_o is a fitted constant indicative of the reinforcement conductivity, p is the reinforcement concentration, p_c is the critical reinforcement concentration for percolation, and t the exponent relating to the matrix microstructure and reinforcement aspect ratio. The best fit values for the conductivity results in Figure 9 estimate the

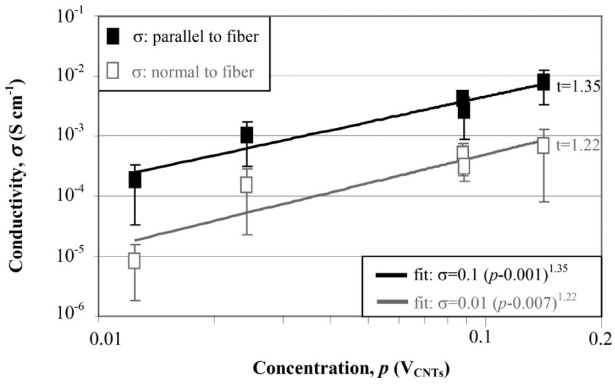

Figure 9. Conductivity normal (■) and normal (□), to the fiber direction for CNT-treated E-glass/epoxy laminates as a function of the CNT-volume fraction (V_{CNTs}) in the laminate.

exponent (t) at 1.35 and 1.2 and a percolation threshold of 0.1 and 0.7% for the parallel and normal directions, respectively.

Previous work has reported values for t between 1.4 and 2 for oxidized, multiwalled CNTs added to an epoxy matrix[65,66] and in the case of polyimide-CNT composites t was 1.6.[67] Similarly, the values for p_c in the epoxy and polyimide nanocomposites were around 0.02%[65] and 0.15%,[67] respectively, indicating that the EPD films formed in this work require similar CNT loading for percolation conductivity to polyimide-CNT nanocomposites. Nanocomposites with higher volume-fractions of CNTs indicate saturation conductivity around 0.05 S cm^{-1} at 5% weight for CNT-epoxy[68] and 0.1 S cm^{-1} at 3.7% volume in CNT-polyimide composites,[67] which compares to 0.01 S.cm^{-1} for the EPD-CNT treated glass/epoxy composites. The reduced saturation conductivity for the CNT film deposited on the glass fibers may be due to the PEI functionalization, which is expected to affect the contact resistance between adjacent CNTs. The overall functionalization process, using the ozone, ultrasonication and PEI, does not appear to be detrimental to the conductivity of the CNT, with σ_0 estimated to be 0.1 S cm^{-1} for the fiber direction, which compares to values between 6×10^{-5} and 5×10^{-3} S cm^{-1} for acid treated[65] and untreated MWCNTs.[67] The specific effect of the ozone and ultrasonication on the intrinsic conductivity of the CNTs cannot be assessed in the present work as the influence of the PEI dendrimers would be expected to dominate the properties of the individual CNT, which is representative of the estimated σ_0 value.

Therefore, the PEI molecules which coat the CNTs and react with the epoxy may produce a wider tunneling junction than in epoxy composites using untreated or oxidized CNTs, if the thermal fluctuation induced tunneling model is applied.[69] Analysis of the data in Figure 9, in which a plot of ln σ vs $p^{-1/3}$ was made (see the Supporting Information, Figure S5), indicated that the linear gradient was a lot shallower than for acid-oxidized and untreated CNTs in epoxy composites.[65] This suggests that the EPD-CNTs are well dispersed even at high concentrations and the flaw density of the matrix and functionalized CNT interfaces is relatively lower. In the current studies, the level of PEI functionalization is tailored for mechanical properties, but future work may be able enhance the electrical conductivity without diminishing mechanical performance.

Interestingly, anisotropy in electrical conductivity, with respect to the fiber direction, was observed. Typically, the

conductivity in the fiber direction was ten times greater than the normal fiber direction (Figure 9). A similar anisotropy has been observed previously for glass/vinyl ester composites containing CNTs in the polymer.[70] In the current work, the anisotropy may be explained on the basis that the CNT-film appears to initially to form along the fiber length and then build up between the fibers (Figures 4 and 5).

Future work may also be able to enhance the thermal conductivity of the laminates by tuning the degree of CNT functionalization. In the present work, we have not assessed the thermal conductivity on the basis of reported measurements on epoxy resins with CNT additives. The modest increases in thermal conduction are believed to be due to the polymer-layer adsorption interfering with the CNT thermal conductivity mechanisms,[71] even for composites with relatively high volume fractions of CNTs.[72]

Figure 10a shows the change in the laminate resistance as a function of applied strain for the ±45° and in-plane shear glass/epoxy laminates with the EPD-CNT treatments. The results indicate that the resistance change, normalized to the specimen width ($\Delta R/L$), increases proportionally with shear strain. A similar resistance change was previously reported for glass/epoxy cross-ply laminates using CNT-modified resin,[23] which was significantly greater than for glass fibers treated with sizing agent containing CNTs.[73] The in-plane shear specimen (Figure 10b) shows an increase in the resistance gradient which may be indicative of increased matrix yielding and damage that occurs in the small overlap region as the specimen approaches failure. The ability to measure very small changes in shear strain may offer a new method to accurately assess shear modulus properties in thin composite specimens or adhesive bondlines. For thin bondlines, accurately measuring adherend displacements as small as 1 μm can be difficult, often leading to considerable error in shear modulus calculations.

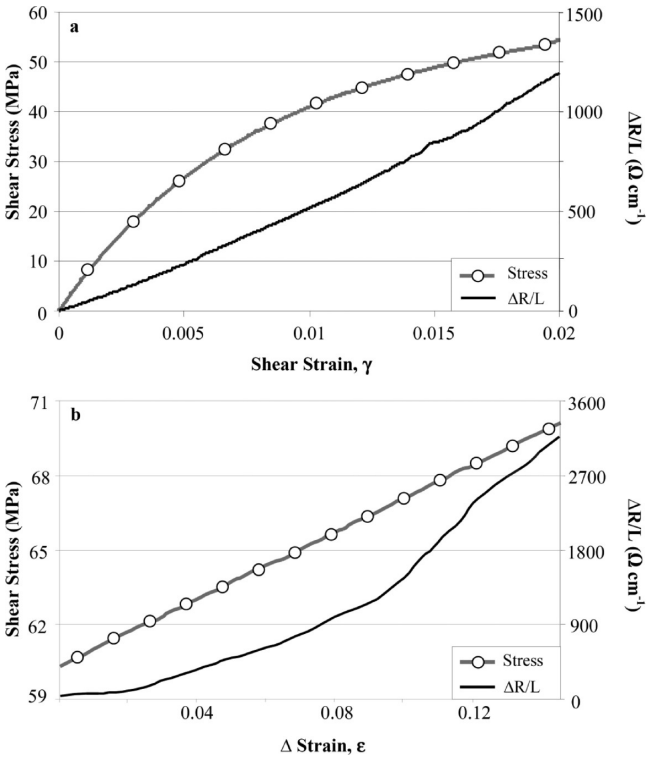

Figure 10. Change in resistance for (a) ± 45° and (b) in-plane shear glass/epoxy laminates with the EPD-CNT treatments, indicating change in resistance with strain compared to the change in shear stress.

4. CONCLUSIONS

Electrophoretic deposition can be successfully applied to coat practical E-glass fabric with high concentrations of CNTs. The functionalization of CNTs using ultrasonication-ozonolysis and PEI provides a dispersion that produces highly uniform depositions of CNTs that chemically link with both the epoxy matrix and sized E-glass fibers in the composite laminates. Considerable increases in the in-plane shear strength of the glass/epoxy laminates resulted from the EPD treatment with CNTs. The increased strength was due to plastic more ductile fracture in the modified-interphase-region that was rich in CNTs. Unmodified laminates, without the hierarchical CNT structure, in contrast, exhibited brittle fracture localized at the glass-epoxy interface. Increases in shear modulus of the composites also corresponded to high levels of CNTs present but heterogeneous distributions of the coating limited increases at the higher CNT concentrations. CNT-modification led to significant increases in laminate conductivity that were comparable to polyimide based nanocomposites and which exhibited anisotropy due to preferential coating of the CNT film in the fiber direction. The CNT-treated laminates also exhibited electrical-resistance sensitivity to applied shear-strain, with the rate of change dependent on the extent of plastic deformation.

■ ASSOCIATED CONTENT

Ⓢ Supporting Information

Shear test specimen dimensions, XPS spectra, cross-sectional optical micrographs, and Halpin−Tsai equations and material property data for modeling. This material is available free of charge via the Internet at http://pubs.acs.org.

■ AUTHOR INFORMATION

Corresponding Author

*E-mail: thosten@udel.edu.

Notes

The authors declare no competing financial interest.

■ ACKNOWLEDGMENTS

This research is funded by National Science Foundation (Grant CMMI-1254540), Dr. Mary Toney, Program Director and the US Army Program Executive Office: Soldier and the Army Research Laboratory and was accomplished under Cooperative Agreement Number W911NF-06-2-011. The authors would like to thank Dr Narelle Brack (La Trobe University) for the XPS measurements.

■ REFERENCES

(1) Drzal, L. T. *Mater. Sci. Eng.* **1990**, *A126*, 289−293.
(2) Sharpe, L. H. *Am. Chem. Soc. Div. Org. Coat. Plast. Chem. Prepr.* **1971**, *31* (2), 201.
(3) Manson, J. A.; Sperling, L. H. *Polymer Blends and Composites*;Plenum Press: NewYork, 1976.
(4) Ishida, H. A. *Polym. Compos.* **1984**, *5*, 101−123.
(5) Korjakin, A.; Rikards, R.; Buchholz, F.-G; Wang, H.; Bledzki, A. K.; Kessler, A. *Polym. Compos.* **1998**, *19* (6), 793−806.
(6) Wang, T. W. H.; Blum, F. D.; Dharani, L. R. *J. Mater. Sci.* **1999**, *34* (19), 4873−4882.
(7) Frenzel, H.; Bunzel, U.; Hassler, R.; Pompe, G. *J. Adhes. Sci. Technol.* **2000**, *14* (5), 651−60.

(8) Plueddemann, E. P. *Silane Coupling Agents*, 2nd ed.; Plenum Press: New York, 1999.
(9) Griswold, C.; Cross, W. M.; Kjerengtroen, L.; Kellar, J. J. *J. Adhes. Sci. Technol.* **2005**, *19* (3−5), 279.
(10) Jensen, R. E.; Palmese, G. R.; McKnight, S. H. *Int. J. Adhes. Adhes.* **2006**, *26* (1−2), 103−115.
(11) Cabibil, H.; Celio, H.; Lozano, J.; White, J. M.; Winter, R.. *Langmuir* **2001**, *17* (7), 2160−2166.
(12) Zhang, C.; Hankett, J.; Chen, Z. *ACS Appl. Mater. Interfaces* **2012**, *4* (7), 3730−3737.
(13) Benkoski, J. J.; Kramer, E. J.; Yim, H.; Kent, M. S.; Hall, J. *Langmuir* **2004**, *20* (8), 3246−3258.
(14) Wang, T. W. H.; Blum, F. D.; Dharani, L. R. *J. Mater. Sci.* **1999**, *34* (19), 4873−4882.
(15) Qian, H.; Greenhalgh, E. S.; Shaffer, M. S. P.; Bismarck, A. *J. Mater. Chem.* **2010**, *20*, 4751−4762.
(16) Diez-Pascual, A. M.; Ashrafi, B.; Naffakh, M.; González-Domínguez, J. M.; et al. *Carbon* **2011**, *49*, 2817−2833.
(17) Shen, Z.; Bateman, S.; Wu, D. Y.; McMahon, P.; Dell'Olio, M.; Gotama, J. *Compos. Sci. Technol.* **2009**, *69*, 239−244.
(18) Zhao, S.; Schadler, L. S.; Duncan, R.; Hillborg, H.; Auletta, T. *Compos. Sci. Technol.* **2008**, *68* (14), 2965−2975.
(19) Chen, C.; Morgan, A. B. *Polymer* **2009**, *50* (26), 6265−6273.
(20) Yavari, F.; Rafiee, M. A.; Rafiee, J.; Yu, Z. Z.; Koratkar, N. *ACS Appl. Mater. Interfaces* **2010**, *2* (10), 2738−2743.
(21) Zhang, X.; Fan, X.; Yan, C.; Li, H.; Zhu, Y.; Li, X.; Yu, L. *ACS Appl. Mater. Interfaces* **2012**, *4* (3), 1543−1552.
(22) Liao, L.; Wang, X.; Fang, P.; Liew, K. M.; Pan, C. *ACS Appl. Mater. Interfaces* **2011**, *3* (2), 534−538.
(23) Thostenson, E. T.; Chou, T. W. *Adv. Mater.* **2006**, *18*, 2837−2841.
(24) Gao, L. M.; Thostenson, E. T.; Zhang, Z. G.; Chou, T.-W. *Adv. Funct. Mater.* **2009**, *19* (1), 123−130.
(25) Pandey, G.; Wolters, M.; Thostenson, E. T.; Heider, D. *Carbon* **2012**, *50* (10), 3816−3825.
(26) Lasater, K. L.; Thostenson, E. T. *Polymer* **2012**, *53* (23), 5367−5374.
(27) Rausch, J.; Mäder, E. *Compos. Sci. Technol.* **2010**, *70*, 1589−1596.
(28) Kim, M.; Park, Y. B.; Okoli, O. I.; Zhang, C. *Compos. Sci. Technol.* **2009**, *69*, 335−342.
(29) Bekyarova, E.; Thostenson, E. T.; Yu, A.; Itkis, M. E.; Fakhrutdinov, D.; Chou, T. W.; Haddon, R. C. *J. Phys. Chem. C* **2007**, *111*, 17865−17871.
(30) Fan, Z.; Santare, M. H.; Advani, S. G. *Compos. Part A.* **2008**, *39* (3), 540.
(31) Thostenson, E. T.; Li, W. Z.; Wang, D. Z.; Ren, Z. F.; Chou, T. W. *J. Appl. Phys.* **2002**, *91* (9), 6034−6037.
(32) Qian, H.; Bismarck, A.; Greenhalgh, E. S.; Shaffer, M. S. P. *Compos. Sci. Technol.* **2010**, *70*, 393−399.
(33) Zhang, Q.; Liu, J.; Sager, R.; Dai, L.; Baur, J. *Compos. Sci. Technol.* **2009**, *69* (5), 594−601.
(34) Kim, K. J.; Yu, W. R.; Youk, J. H.; Lee, J. *ACS Appl. Mater. Interfaces* **2012**, *4* (4), 2250−2258.
(35) Boccaccini, A. R.; Roether, J. A.; Thomas, B. J. C.; Shaffer, M. S. P. *J. Ceram. Soc. Jpn.* **2006**, *114* (1), 1−14.
(36) Boccaccini, A. R.; Cho, J.; Roether, J. A.; Thomas, B. J. C.; Minay, E. J.; Shaffer, M. S. P. *Carbon* **2006**, *44*, 3149−3160.
(37) Boccaccini, A. R.; Cho, J.; Subhani, T.; Kaya, C.; Kaya, F. *J. Eur. Ceram. Soc.* **2010**, *30*, 1115−1129.
(38) Van der Biest, O. O.; Vandeperre, L. J. *Annu. Rev. Mater. Sci.* **1999**, *29*, 327−352.
(39) Bekyarova, E.; Thostenson, E. T.; Yu, A.; Kim, H.; Gao, J.; Tang, J. *Langmuir* **2007**, *23* (7), 3970−3974.
(40) Lee, S.; Choi, O.; Lee, W.; Yi, J.; Kim, B.; Byun, J.; Yoon, M,-K.; Fong, H.; Thostenson, E. T.; Chou, T.-W. *Compos. Part A* **2011**, *42*, 337−344.
(41) An, Q.; Rider, A. N.; Thostenson, E. T. *Carbon* **2012**, *50* (11), 4130−4143.
(42) *ASTM D3846: Standard test Method for In-Plane Shear Strength of Reinforced Plastics*; American Society for Testing and Materials: West Conshohocken, PA, 2002.
(43) *ASTM D3518: In-Plane Shear Response of Polymer Matrix Composite Materials by Tensile Test of a ±45° Laminate*; American Society for Testing and Materials: West Conshohocken, PA, 2001.
(44) *ASTM D1505: Test Method for Density of Plastics by the Density-Gradient Technique*; American Society for Testing and Materials: West Conshohocken, PA, 2003.
(45) *ASTM Standard D3171: Standard Test Methods for Constituent Content of Composite Materials*; American Society for Testing and Materials: West Conshohocken, PA, 2006.
(46) *ASTM D257: Standard Test Methods for DC Resistance or Conductance of Insulating Materials*; American Society for Testing and Materials: West Conshohocken, PA, 2006.
(47) Woo, H.; Reucroft, P. J.; Jacob, R. J. *J. Adhesion Sci. Technol.* **1993**, *7* (7), 681−697.
(48) Liu, L.; Hu, J-.M.; Zhang, J-.Q.; Cao, C. N. *Electrochim. Acta* **2006**, *52*, 538−545.
(49) Sun, J.; Gao, L. *Carbon* **2003**, *41* (5), 1063−1068.
(50) Chen, Q.; Boothroyd, C.; Soutar, A. M.; Zeng, X. T. *J. Sol−Gel Sci. Technol.* **2010**, *53* (1), 115−120.
(51) Plonka, R.; Mader, E.; Gao, S. L.; Bellmann, C.; Dutschk, V.; Zhandarov, S. *Compos. Part A* **2004**, *35*, 1207−1216.
(52) Briggs, D.; Beamson, G. *High-Resolution XPS of Organic Polymers: the Scienta ESCA300 Database*; Wiley: New York, 1992.
(53) Segut, O.; Herlem, G.; Lakard, B.; Blondeau-Patissier, V.; Nardin, M.; Gree, S. *Syn Met.* **2010**, *160*, 1359−1364.
(54) Finšgar, M.; Fassbender, S.; Nicolini, F.; Milošev, I. *Corros. Sci.* **2009**, *51*, 525−533.
(55) Burg, P.; Fydrych, P.; Cagniant, D.; Gerard, N.; Bimer, J.; Jankowsa, A. *Carbon* **2002**, *40*, 1521−1531.
(56) Hamaker, H. C. *Trans. Faraday. Soc.* **1940**, *36*, 279−287.
(57) Zhitomirsky, I. *J. Mater.Sci.* **2006**, *41*, 8186−8195.
(58) Nguyen, F. N.; Saks, A. M.; Berg, J. C. *J. Adhesion Sci. Technol.* **2007**, *21* (14), 1375−1393.
(59) Sun, L.; Warren, G. L.; O'Reilly, J. Y.; Everett, W. N.; Lee, S. M.; Davis, D.; Lagoudas, D.; Sue, H.-J. *Carbon* **2008**, *46*, 320−328.
(60) Halpin, J. C. *J. Compos. Mater.* **1969**, *3*, 732−734.
(61) Yeh, M.-K.; Tai, N.-H.; Liu, J-H. *Carbon* **2006**, *44*, 1−9.
(62) Luciano, R.; Barbero, E. J. *Int. J. Solids Struct.* **1994**, *31*, 2933−2944.
(63) Kim, M.; Park, Y.-B.; Okoli, O.; Zhang, C. *Compos. Sci. Technol.* **2009**, *69*, 335−342.
(64) Stauffer, D. *Introduction to the Percolation Theory*; Francis and Taylor: London, 1991.
(65) Kim, Y. J.; Shin, T. S.; Choi, H. D.; Kwon, J. H.; Chung, Y. -C.; Yoon, H. G. *Carbon* **2005**, *43*, 23−30.
(66) Barrau, S.; Demont, P.; Peigney, A.; Laurent, C.; Lacabanne, C. *Macromolecules* **2003**, *36*, 5187−5194.
(67) Jiang, X.; Bin, Y.; Matsuo, M. *Polymer* **2005**, *46*, 7418−7424.
(68) Thostenson, E. T.; Chou, T.-W. *Carbon.* **2006**, *44*, 3022−3029.
(69) Sheng, P. *Phys. Rev. B* **1980**, *21* (6), 2180−2195.
(70) Thostenson, E. T.; Gangloff, J. J.; Li, C.; Byun, J-.H. *Appl. Phys. Lett.* **2009**, *95*, 073111.
(71) Gojny, F. H.; Wichmann, M. H.G.; Fiedler, B.; Kinloch, I. A.; Bauhofer, W.; Windle, A. H.; Schulte, K. *Polymer.* **2006**, 2036−2045.
(72) Yamamoto, N.; de Villoria, R. G.; Wardle, B. L. *Compos. Sci. Technol.* **2012**, *72*, 2009−2015.
(73) Gao, L.; Chou, T. W.; Thostenson, E. T.; Zhang, Z. *Carbon* **2010**, 3788−3794.